Transient Response Evaluation of a Hydraulic Engine Mount

R. Singh, H. Adiguna and **M. Tiwari**, The Ohio State University, Columbus, Ohio
H. Tseng and **D. Hrovat**, Ford Motor Company, Dearborn, Michigan

The transient response of a typical hydraulic engine mount has been studied using analytical and experimental methods. First, a lumped parameter nonlinear model is used to formulate the problem and to suggest parameters that must be experimentally determined. Several configurations related to inertia track and decoupler are analyzed. Next, two bench experiments are constructed for the identification of nonlinear chamber compliances (with and without preloads) and nonlinear fluid resistances. The nonlinear characteristics of the decoupler are described to accurately predict the time events of the decoupler gap opening and closing. An equivalent viscous damper model is employed along with a multistaged switching mechanism. Nonlinear behavior caused by the vacuum formation in the top chamber is studied by defining a bilinear asymmetric stiffness curve. All governing equations are then solved in the time domain to yield responses when step up, step down or triangular displacement waveforms are applied. New transient experiments were also conducted with an elastomer test system by applying known displacement inputs. Measured transmitted force and top chamber pressure signals were analyzed in the time and frequency domains. Results of the proposed simulation model match well with measured data.

Hydraulic engine mounts such as the units shown in Figure 1 are designed and tuned to provide amplitude-sensitive and spectrally varying properties.[1-5] Performance is typically measured on a steady state basis using the sinusoidal nonresonant-type test method[2-4] currently employed for product design and quality control. Nevertheless, their transient characteristics are poorly understood and relevant simulation methods or experimental techniques are not readily available. Therefore, the chief objective of this article is to summarize simulation models that may be utilized to design, specify and diagnose transient characteristics due to many vehicle conditions such as travel on bumpy roads, abrupt accelerations or decelerations, garage shift events, braking and cornering.

Simulation Model

The concept of a hydraulic mount is illustrated in Figure 2 where $u(x,t)$ is the hydraulic reaction force. Here, the terms q_i, q_d, p_1, p_2, $\bar{p}$, x, A_p and F_T denote the flow rate through inertia track (#i), flow rate through decoupler (#d), top chamber (#1) pressure, bottom chamber (#2) pressure, pressure at the static equilibrium condition, displacement excitation, equivalent piston area and transmitted force, respectively. The mount is modeled by lumping the fluid system into several control volumes as shown in Figure 3. The system parameters include the top and bottom chamber fluid compliances (C_1 and C_2), elastomeric element stiffness (k_r) and damping (b_r), inertia track inertance (I_i) and fluid resistance (R_i) and decoupler resistance (R_d). Through experimentation, it is shown that C_1, C_2, R_i and R_d have nonlinear characteristics.[2,4] The momentum and continuity equations yield the following equations; refer to References 1-5 for details.

$$q_i(t)+q_d(t)=A_p\dot{x}(t)-C_1(p_1)\dot{p}_1(t) \tag{1}$$

$$-q_i(t)-q_d(t)=C_2(p_2)\dot{p}_2(t) \tag{2}$$

$$F_T(t)=b_r\dot{x}(t)+k_r x(t)+A_p(\bar{p}-p_1(t)) \tag{3}$$

The inertia track is modeled by the following differential equation where the R_i term depends on fluid variables.

$$I_i\dot{q}_i(t)+R_i(\Delta p_{12},q_i)q_i(t)=p_2(t)-p_1(t)=\Delta p_{12}(t) \tag{4}$$

In general, the relation between steady state pressure drop (Δp_{12}) and steady flow rate (q_i) in a pipe is nonlinear:

$$q_i=C_d A_i\sqrt{2\Delta p_{12}/\rho}$$

where C_d is the coefficient of discharge. In our work, R_i is determined via a bench experiment.[2,4] For the case of a free floating decoupler, the fluid flow is controlled by the decoupler switching mechanism which couples or decouples the inertia track. On the other hand, when the disk is at the top or at the bottom, q_d is zero and thus the fluid can only flow through the inertia track. A linear model of the decoupler is given by a first order differential Equation (5) where b_v and A_d denote the viscous damping coefficient and cross-sectional area of the decoupler gap, respectively. Further, m_d and x_d represent the disk mass and displacement of the decoupler.

$$m_d\ddot{x}_d(t)+b_v\dot{x}_d(t)=A_d[p_2(t)-p_1(t)];\ \dot{x}_d(t)=\frac{q_d(t)}{A_d} \tag{5a-b}$$

Experimentally, the dynamics of the decoupler are studied by installing a pressure transducer in the top chamber as shown in Figure 4. The closing and opening events of the decoupler can be clearly observed from the top chamber pressure $p_1(t)$ time history.

A nonlinear simulation model using MATLAB/Simulink was developed. Except for the decoupler, nonlinear components can be modeled via continuous nonlinear functions. Such continuous relationships are obtained either experimentally or via mathematical descriptions of the physical processes. Some nonlinearities can be linearized provided the dynamic excursion range is small. This holds true for $p_2(t)$ because C_2 is very high and the associated dynamic excursions are close to the atmospheric pressure. In addition, the top pressure chamber exhibits an asymmetric nonlinearity because of the vacuum formation. Nevertheless, the stiffness in both regimes was treated as linear with very different slopes and the transition at $p_1 = p_a$ is assumed continuous. In some cases, a polynomial curvefit was employed. The nonlinear model was solved employing the 4th order Runge-Kutta method with a fixed time step. The total time to run the steady state simulation model for a particular X and f of excitation was specified by $60T$ where $T = 1/f$ is the period of excitation. Of the $60T$ time span, the first $40T$ was used to overcome starting transient effects. Data from the rest of the time ($20T$) was used for time or frequency domain validation processes. The free decoupler model consumed more time due to the additional nonlinearity introduced by the decoupler mechanism.

A comparison of experimental results between the fixed ($R_d \to \infty$) and free decoupler (finite R_d) cases showed that the nonlinearity is caused mostly by the vacuum pressure created in the top chamber and the decoupler switching action. The elimination of the decoupler focused the study on the formation of the vacuum, which is still poorly understood. The initial conditions for $p_1(t)$ and $p_2(t)$ were set as atmospheric pressure p_a. Since the compliance of each chamber is nonlinear at each time step, the operating pressure was used to estimate C_1 and C_2 from the measured p-V curves. Each compliance (C_1 or C_2) was expressed as a polynomial function of pressure (p_1 or

p_2). The dynamic pressures $p_1(t)$ and $p_2(t)$ calculated throughout the simulation are gage pressures (above or below p_a). The inertia track subsystem is constructed based on Equation (4). The Δp_{12} due to R_i element is utilized as a feedback loop to this system. The nonlinear resistance R_i is specified as a function of q_i. The initial condition for q_i is zero since the simulation is assumed to start from the static equilibrium condition. The transmitted force subsystem calculates the components contributed by both rubber and fluid elements, as shown by Equation (3). The rubber stiffness k_r and damping b_r are interpolated from measured data by employing a look-up table, while p_1 is calculated numerically from the top chamber subsystem.

In the free decoupler model, yet another subsystem associated with a free-floating disk is integrated in the mount model. The equation for motion for the decoupler gap is based on Equation (5) derived for the dashpot model. The decoupler subsystem has to be enabled or disabled depending whether the decoupler opens or closes. The states of the system such as $\dot{x}_d$ and x_d have to be held or reset to zero whenever the decoupler closes.

To better understand the phenomenon, the sequence of events is divided into 5 stages:

Stage 1 – Initially, the disk is assumed to be at the top ($x_d = D_d$) and the gap is closed and hence $q_d = 0$ and $q = q_i$.

Stage 2 – When $p_1 > p_2$, the decoupler starts to move down (open) and as a result, the fluid flow through the decoupler q_d tries to equalize the p_1 and p_2 and oppose an increase in p_1. Notice that q_i is still >0 although the disk is moving downward. This is due to the inertance effect of the inertia track.

Stage 3 – The disk is at the bottom ($x_d = 0$) and the decoupler gap is closed ($q_d = 0$). Due to the decreasing q_i, p_1 increases. Then q_i changes direction, which causes p_1 to decrease.

Stage 4 – When $p_1 < p_2$, the disk starts to move up (gap is now open) and the p_1 suddenly stops varying until the decoupler is closed again.

Stage 5 – The decoupler disk is at the top and as $x(t)$ and q_i move upward, vacuum is now generated. During this stage, $p_1 < p_2$ and $p_1 < p_a$. When $x(t)$ changes direction, p_1 again starts to increase. Stages 2 to 5 continue to repeat themselves.

Experimental Methodology

Bench experiments were constructed to study the nonlinear characteristics of C_1, C_2 and R_i. The objectives of these experiments were to determine whether the nonlinear characteristics can be modeled by simplified theoretical expressions. Alternatively, empirical results must be incorporated in simulation. Sinusoidal or transient dynamic tests have been done using the MTS (Model 831.50, 1000 Hz) elastomer test system (see Figure 4).[4] Two configurations of the take-apart mount are used for study: (a) free decoupler mount with both decoupler and inertia track; and (b) fixed decoupler mount without any decoupler. The take-apart mount was assembled in a water bath so as not to include any air. The assembly was done with a clamping fixture. Care needed to be taken that there were no bubbles in the water bath, which can be trapped during the assembly of the mount. To maintain a low level of dissolved air, the water temperature was kept low. The internal dynamics were studied by installing a pressure transducer in the top chamber as shown in Figure 5 and measuring the dynamic pressure $p_1(t)$. This could accurately map the dynamic stages of the decoupler as the $p_1(t)$ waveform gives a very good understanding of the internal dynamics. Two kinds of pressure transducers were used for experimentation: (a) an absolute pressure transducer (strain gage); and (b) a dynamic pressure transducer (piezoelectric). The absolute pressure transducer was primarily used for recording the mean $\bar{p}_1$ level while the dynamic pressure transducer was used for accurately recording $p_1(t)$. Under the static manual control of the MTS controller, the mount was subjected to varying loads and $\bar{p}_1$ was recorded. This gave an estimate of the initial pressure to be used for simulation.

A transient displacement input $x(t)$ was applied to the mount using the MTS system. The servohydraulic system was programmed in the displacement control mode for applying single 'rectangular' (step up and step down), triangular and sawtooth waveforms. All such excitations were applied over a mean displacement input x_m corresponding to $F_m = -1200$ N. The top chamber pressure $p_1(t)$, transmitted force $F_t(t)$ and displacement excitation $x(t)$ signals were acquired and processed using the digital system that is independent of the MTS machine.

Transient Response

Transient response simulations were conducted by applying step and pulse displacement inputs corresponding to the experimental waveforms. For example, Figure 6 shows the measured waveforms corresponding to step-up and down transients. The step-up displacements of Figures 6-8 are obtained by applying a 1200 N (say *B*) compressive preload and then releasing it to 0 N (say *A*). The procedure is reversed for step down (Figure 6). The forces transmitted by the mount for step-up and step-down displacements are different. The $F_T(t)$ peak during the step up (*B* to *A*) is less than the force transmitted during the step down (*A* to *B*) as shown in Figure 6. This further strengthens our claim that the mount behaves in an asymmetric manner. The role of vacuum formation is very dominant in controlling such an asymmetric behavior.

For the step input (Figures 7 and 9), measured F_T and p_1 values show a faster decay than predicted results. This might be caused by the unmodeled dynamics associated with the inertia track. The period of the decaying oscillations is smaller for the simulation. This might be due to the amplitude and frequency dependence of C_1. The vacuum formation reduces the expected overshoot for both simulation and experiment. An impulse input to the mount is difficult to experimentally achieve and therefore a triangular waveform was used. This input, as shown in Figures 8 and 10, is acquired by applying a preload B = 1200 N, releasing to A = 0 N in 0.1 sec and compressing it again to *B* in yet another 0.1 sec while subjecting the mount to a gradual ramp input (Figures 8 and 10). There is a limit to the pulse width that can be achieved by a servo-hydraulic test system. Further, a reduction in the pulse time makes it difficult to achieve the peak amplitude. Figures 8 and 10 show that the transmitted force $F_T(t)$ and top chamber pressure $p_1(t)$ from simulation and experiment match very well although predictions show less damping and a slower decay of oscillations.

For the free decoupler case, q_i, q_d, and x_d time histories are plotted for a better understanding of the inertia track dynamics and the decoupler switching mechanism. Figure 6 shows that, when compared to the case of fixed decoupler (Figure 4), the addition of a free decoupler results in reduced oscillations. This suggests that the decoupler introduces damping to the system. Decoupler action comes out very prominently in the simulated waveforms (Figures 9 and 10) of p_1 and F_T. As the decoupler closes, p_1 rises significantly as shown by the small 'bumps.' The disk displacement x_d is also plotted to illustrate the sequencing mechanism. One final note regarding the measured $p_1(t)$ histories is that p_1 is measured using a dynamic transducer with a lower frequency limit of 0.5 Hz. Consequently, measured results show a very low frequency trend or drift. Such trends are not obviously seen in simulations.

Conclusion

The dynamic response of a typical hydraulic engine mount to transient excitations has been theoretically and experimentally analyzed. This work is new and in the process and we had to investigate the steady state behavior as well. New dynamic experiments have also been conducted given step, pulse (triangle) and sawtooth displacement profiles. A new switching model of the decoupler based on an equivalent viscous damping mechanism concept is used and this formulation matches well with transient measurements. The proposed simulation model can be integrated within a larger vehicle dynamic model. Finally, the experimental procedure we have used could lead

to a standard transient test and correlation method with real-life events.

Acknowledgment

We gratefully acknowledge research support from the Ford Motor Company. Experimental studies were made possible by equipment grants from the Ohio Board of Regents and the MTS Systems Corporation. Finally, we acknowledge Delphi Automotive (Chassis) for supplying the mounts.

References

1. R. Singh, G. Kim, and P. V. Ravindra, "Linear Analysis of Automotive Hydro-mechanical Mount with Emphasis on Decoupler Characteristics," *Journal of Sound and Vibration*, 158(2), 219-243, 1992.
2. G. Kim, and R. Singh, "Nonlinear Analysis of Automotive Hydraulic Engine Mount," *ASME Journal of Dynamic Systems, Measurement and Control*, 115, 482-487, 1993.
3. G. Kim, and R. Singh, "Study of Passive and Adaptive Hydraulic Engine Mount Systems with Emphasis on Nonlinear Characteristics," *Journal of Sound and Vibration*, 179(3), 427-453, 1995.
4. M. Tiwari, H. Adiguna, and R. Singh, "Experimental characterization of a Nonlinear Hydraulic Engine Mount," submitted to the *Noise Control Engineering Journal*, 2002.
5. H. Adiguna, M. Tiwari, R. Singh, H. E. Tseng, and D. Hrovat, "Transient Response of a Hydraulic Engine Mount," submitted to the *Journal of Sound and Vibration*, 2002.

The authors can be contacted at: singh3@osu.edu.

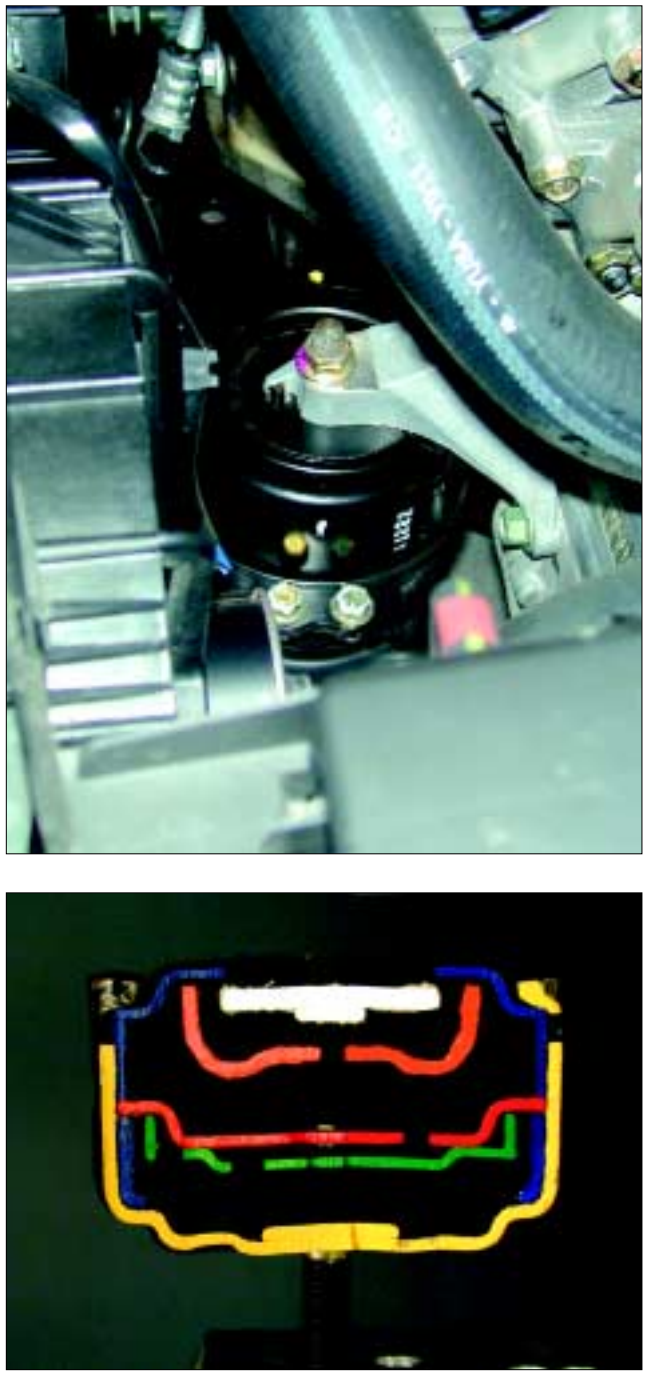

Figure 1. Hydraulic engine mount in an automobile and cutaway view of a typical unit.

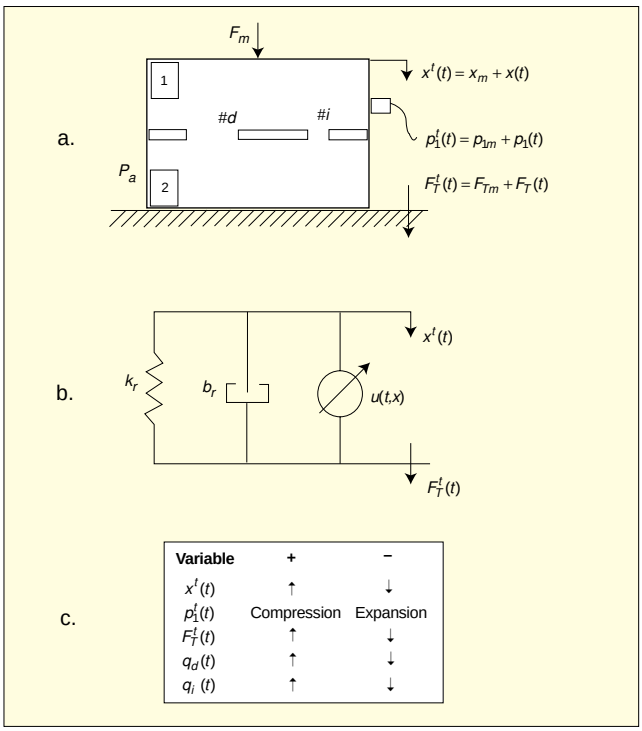

Figure 2. Hydraulic mount concept: (a) measured variables; (b) force transmission paths; (c) sign convention where ↑ implies an upward motion and ↓ refers to a downward motion.

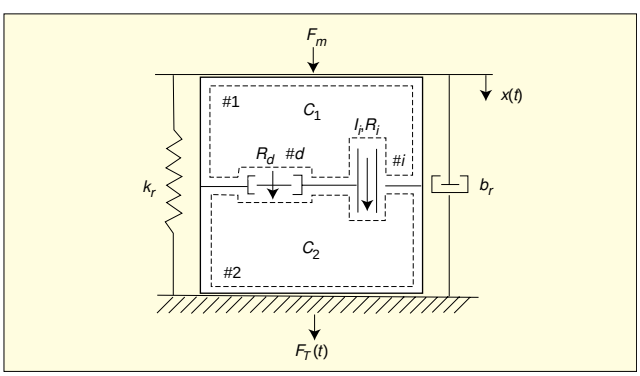

Figure 3. Lumped parameter model of a hydraulic engine mount.

Figure 4. MTS elastomer testing system being used to evaluate the dynamic characteristics of a hydraulic engine mount.

Figure 5. Dynamic pressure transducer installed in the top chamber of a hydraulic engine mount.

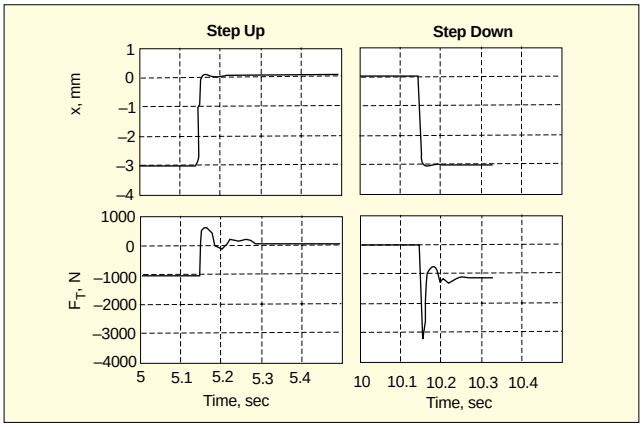

Figure 6. Measured step-up and step-down displacement excitation and transmitted force waveforms for a free decoupler mount.

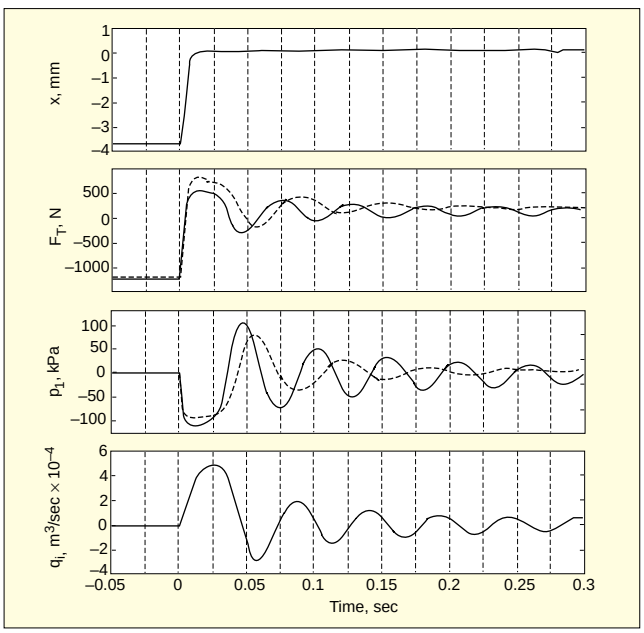

Figure 7. Step response of the fixed decoupler mount (simulations shown as solid plots and measured values shown as dashed plots for F_T and p_1 parameters).

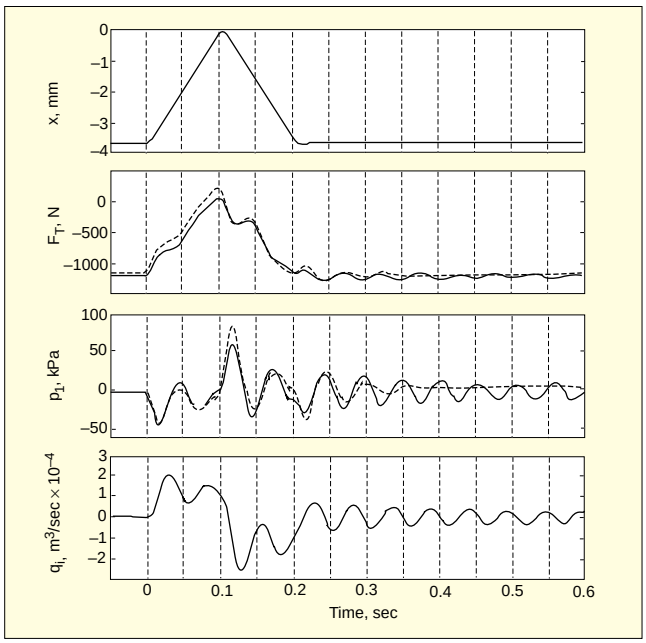

Figure 8. Pulse response of the fixed decoupler mount (simulations shown as solid plots and measured values shown as dashed plots for F_T and p_1 parameters).

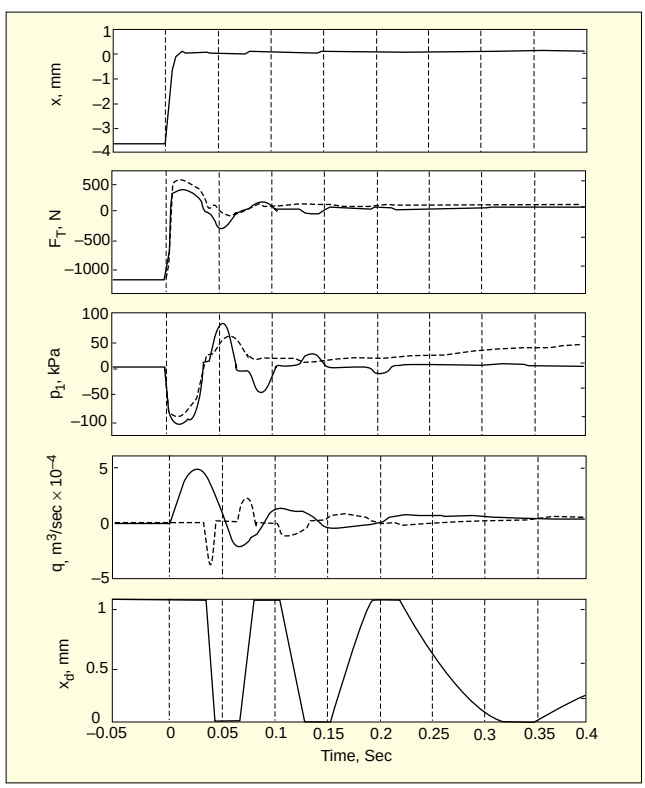

Figure 9. Step response of the free decoupler mount (simulations shown as solid plots and measured values shown as dashed plots).

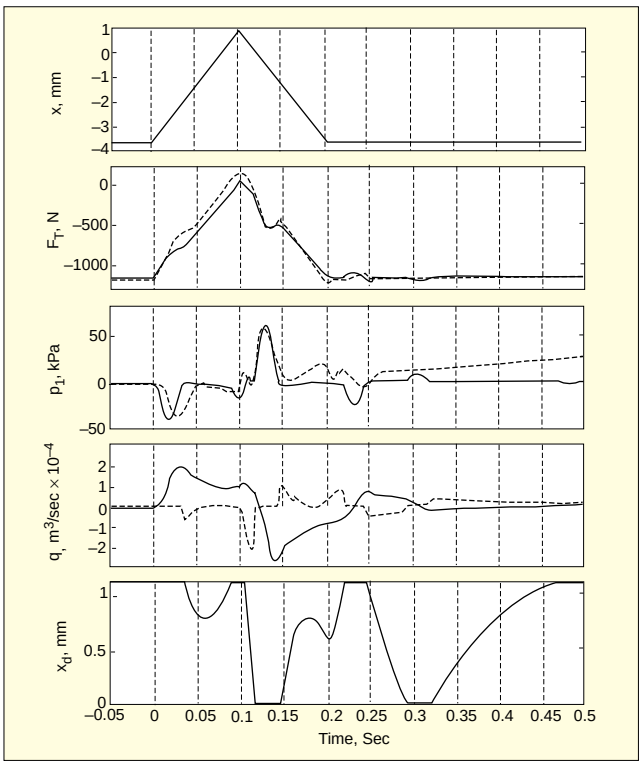

Figure 10. Pulse response of the free decoupler mount (simulations shown as solid plots and measured values shown as dashed plots).

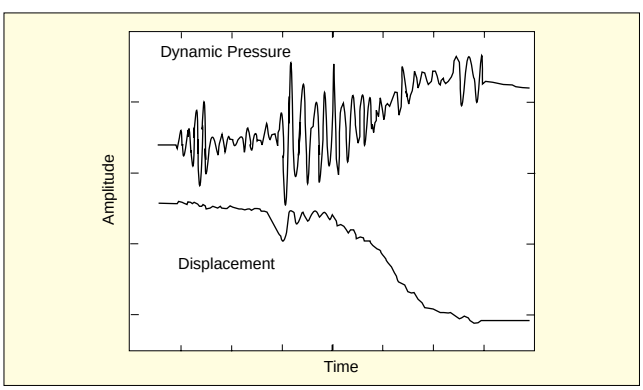

Figure x. Comparison of dynamic pressure response vs. displacement of a hydraulic engine mount.